Measuring Massive Metastable Charged Particles with ATLAS RPC Timing Information

John Ellis[1] Are R. Raklev[2,3] Ola K. Øye[4]

1) Theory Division, Physics Department, CERN, CH-1211 Genève, Switzerland
2) DAMTP, CMS, Wilberforce Road, Cambridge CB3 0WA, UK
3) Cavendish Laboratory, J.J. Thompson Avenue, Cambridge CB3 0HE, UK
4) Department of Physics and Technology, University of Bergen, N-5007 Bergen, Norway

Abstract

We investigate the measurement of massive metastable charged particles in ATLAS, using timing information from the resistive plate chambers (RPCs). As representative particle candidates we use staus, the partners of τ leptons in supersymmetric models with gravitino dark matter (GDM), which may well be stable on the scale of the detector. The generic signatures of massive metastable charged particles are a long Time-of-Flight (ToF) and high energy-loss (dE/dx). The RPC timing information allows us to measure the ToF of a particle which, taken in conjunction with the measurement of the particle's momentum from its track, allows one to determine its mass. We pioneer the study of the RPCs' potential for this measurement. We also consider triggering effects on the event selection, and discuss quantitatively the ATLAS potential for measuring the stau mass in three specific GDM benchmark scenarios.

ATL-PHYS-PUB-2007-016
12 October 2007

1 Introduction

In preparation for the start-up of the LHC, the possible signatures of supersymmetric models have received much attention. This effort has been motivated by the possible benefits of supersymmetric models, including less fine-tuning for the Higgs mass [1–3], the unification of forces at some high scale [4–7], and a viable cold dark matter (CDM) candidate [8, 9] if R-parity is conserved. While most scenarios considered have dealt with minimal versions of supersymmetry, such as the constrained minimal supersymmetric extension of the Standard Model (CMSSM), and have focused on neutralino dark matter candidates, there exist other generic possibilities. One such possibility is gravitino dark matter, in which case heavier metastable charged particles might be produced at the LHC. There are models in which the lifetime of the next-to-lightest supersymmetric particle (NLSP) is longer than it takes to traverse a detector, after which it decays into the neutral lightest supersymmetric particle (LSP), the cold dark matter candidate. Prominent examples of such models include gauge-mediated supersymmetry breaking (GMSB) [10–16], anomaly-mediated supersymmetry breaking (AMSB) [17,18] and supergravity scenarios with gravitino dark matter (GDM) [19–34]. A generic possibility is that the NLSP has electric charge, as is the case for the supersymmetric partner of the tau lepton, the stau ($\tilde{\tau}$). In addition to this example, there are certainly many more models with massive metastable charged particles, both supersymmetric and non-supersymmetric, motivating an investigation of the ATLAS potential for discovering and for measuring the masses of particles in this class of models.

Whilst most R-parity-conserving supersymmetry models studied to date have signatures of large amounts of missing energy from the escaping dark matter candidates, the models with massive metastable charged particles have instead distinctive Time-of-Flight (ToF) and energy-loss (dE/dx) signatures for the NLSPs. In these R-parity-conserving models, supersymmetric particles are produced in pairs, with each one leading via its decay chain to one of the NLSPs. If long-lived, charged, not strongly-interacting and sufficiently energetic to escape the detector, these will appear as a pair of anomalous tracks in the ATLAS muon system, with a significant fraction displaying velocities inconsistent with muons. The difference between the NLSP mass and that of the muon will also result in characteristic differences in energy loss due to ionisation.

In this note we utilise the potential of the resistive plate chambers (RPCs) of the ATLAS muon system for measuring the ToF of massive metastable charged particles. By using the RPCs' timing information for tracks reconstructed in the muon system, and their distance from the interaction point, the particle velocity can be found. The ToF measurement can be calibrated to correct for signal propagation delays in the RPCs, and the flight length can be adjusted to account for the bending of the track in the magnetic field. The resulting velocity can be compared to the momentum measured for the track, and an estimate of the particle mass is obtained from the well known formula

$$m = \frac{p}{\beta\gamma}. \tag{1}$$

We discuss the efficiency of the ATLAS Level 1 triggers for retaining events containing metastable staus, how to isolate their tracks from the background of muon tracks, and how to perform statistical measurements of their masses in three GDM scenarios. A similar analysis of the potential of the ATLAS muon system has been carried out in [35, 36], using the monitored drift tubes (MDTs), and looking at the fit quality of tracks as a function of the particle's assumed arrival time in the MDTs. Our study is complementary to this, and a final analysis of data could benefit from a combination of the two.

As representatives of models with massive metastable charged particles we use the set of gravitino dark matter (GDM) benchmark points (ϵ, ζ, η) proposed in [37]. The benchmark points are based on minimal supergravity models with a specific choice for the trilinear parameter A_0, as found in the Polonyi model of supersymmetry breaking in a hidden sector [38]. The points feature the stau NLSP as the massive metastable charged particle, with lifetimes above 10^4 s for all three benchmark points. From the ATLAS point of view, the ϵ benchmark point is an optimal scenario, featuring light supersymmetric partners, a stau with a nominal mass $m_{\tilde{\tau}_1} = 152.475$ GeV, and a relatively large total supersymmetric cross sections at the LHC of 3.35 pb at next-to-leading order [39], with dominant squark-gluino production. The ζ and η points are less favourable for the LHC, with nominal stau masses of $m_{\tilde{\tau}_1} = 338.114$ GeV and $m_{\tilde{\tau}_1} = 318.931$ GeV and total cross sections of 23.4 fb and 24.1 fb, respectively. For the ζ and η benchmark points, the total cross sections have significant contributions from Drell-Yan production of stau pairs and associated production of chargino-neuralino pairs. For further details on the benchmarks the reader is referred to [37, 39]. We have previously studied the LHC potential for measuring the masses of the spectra of heavier sparticles in [39], using a fast simulation of a generic LHC detector.

Although the analysis described here is carried out for staus in GDM models, the results of the detector simulation should have a more generic applicability to many species of massive metastable charged particles without strong interactions. The spread in stau masses and production processes make these benchmark points a good choice for exploring the ATLAS potential for massive metastable charged particles.

We begin in Section 2 by giving an overview of the simulation we have carried out, before discussing the Level 1 trigger efficiency for the GDM scenarios in Section 3. In Section 4 we go

on to discuss the reconstruction efficiency of stau tracks in the muon system, and in Section 5 we deal with the momentum measurement. Section 6 covers the central topic of our note, namely the ToF measurement of reconstructed stau tracks using RPCs. The potential of using the long ToF of staus as a cut on the Standard Model (SM) background is evaluated in Section 7. Finally, we discuss in Section 8 the accuracy obtainable on the mass of the stau from momentum and ToF measurements, before we draw our conclusions in Section 9.

2 Overview of the Simulation

As the prime example of the potential value added by the ATLAS RPCs, we have selected the ϵ benchmark point proposed in [37]. For this example, we have generated 10025 SUSY events, corresponding to an integrated luminosity of 3.01 fb^{-1}, using `PYTHIA 6.403` [40] and the CTEQ 5L parton distribution functions [41]. The decay widths and branching ratios of the sparticles have been calculated using `SDECAY 1.1a` [42]. For the ζ and η benchmarks, we have generated 9775 and 8075 events, corresponding to integrated luminosities of 419 fb^{-1} and 334 fb^{-1}, respectively. The event generation was performed using ATLAS release 12.0.6 and production cache 12.0.6.4, using the job transform `csc_evgen.trf` with the jobOptions `DC3.006630.MMCP_epsilon.py`, `DC3.006631.MMCP_zeta.py` and `DC3.006632.MMCP_eta.py` found in the package `DC3_jobOptions`.

For later reference, we show in Fig. 1 the Monte Carlo (MC) truth distributions for the velocity and rapidity of the $\tilde{\tau}$ NLSP for the three benchmark points. In Fig. 2 we display these distributions for the ϵ benchmark alone, separating by different production processes. Each distribution is normalised to unity.

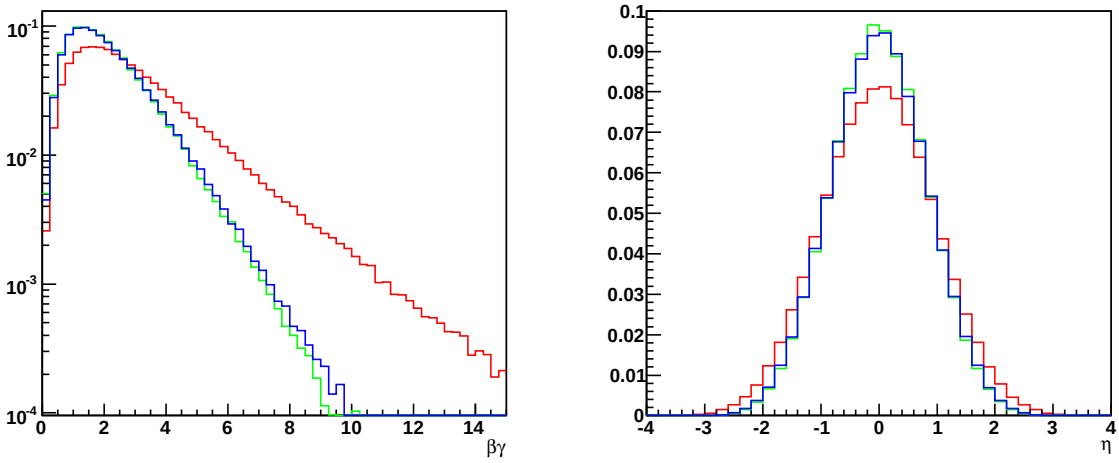

Figure 1: The MC truth distributions of $\beta\gamma$ (left) and rapidity η (right) for staus in the ϵ (red), ζ (green) and η (blue) benchmark points.

We note that the $\beta\gamma$ and η distributions for scenario ϵ are somewhat broader than those for scenarios ζ and η. These reflect the lighter sparticle masses in the ϵ scenario, and the different production mechanisms, as is apparent from Fig. 2 (left) where we see the softer spectrum resulting from the Drell-Yan production of staus.

The results of the full detector simulation and reconstruction have been obtained from the current understanding of the ATLAS detector contained within the `ATHENA` framework [43]. All simulation and reconstruction were run using ATLAS release 12.0.6 and detector description

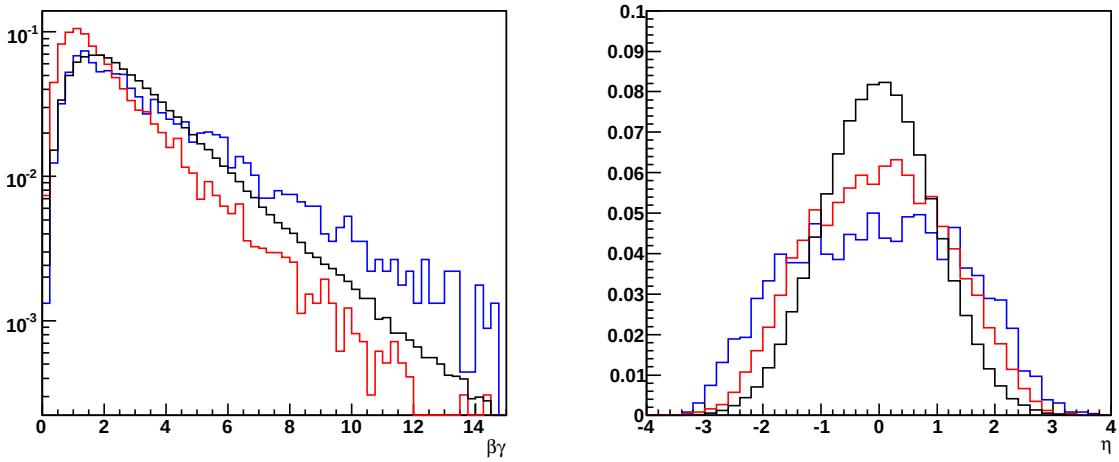

Figure 2: The MC truth distributions of $\beta\gamma$ (left) and pseudo-rapidity η (right) for staus produced in the ϵ benchmark scenario via the Drell-Yan mechanism (red), associated chargino/neutralino production (blue) and other supersymmetric events (black).

`ATLAS-CSC-01-02-00`, including both material and field distortions. For executing simulation and reconstruction, the transforms `csc_simul_trf.py` and `csc_recoESD_trf.py` from production cache 12.0.6.4 were used.

No model for stau energy deposition is included in GEANT4 by default. Therefore, the external GEANT4 module `Sleptons` is used for this purpose.[1] The mechanisms for stau interactions included in this module are ionisation, as calculated from the Bethe-Bloch formula, and multiple scattering. GEANT4's own implementations of these mechanisms are used.

For the reconstruction of the stau tracks, we use the MOORE tracking algorithm in the muon system, and the MuID package for combining MOORE tracks with tracks from the Inner Detector (ID). This was run with the default settings of `ATLAS 12.0.6`.

As the ATLAS detector converges on its start-up state, the hardware and geometry may still undergo minor changes, and the software will remain under continuous development. Nevertheless, we believe that the results presented in the following Sections represent quite reliably the accuracy achievable with the ATLAS detector for the measurement of staus during the first years of LHC running using RPC timing information.

3 Simulation of the Triggers

A crucial piece of information is the efficiency with which ATLAS can trigger on supersymmetric events with metastable staus. One expects good trigger efficiencies in general for events with the production of heavy strongly-interacting supersymmetric particles decaying in cascade decays, which are likely to result in energetic jets, leptons and missing energy [2].

The ATLAS trigger system consists of three levels of triggers. We only take into account the lowest level, Level 1 (LVL1), in this study, since the Level 2 triggers in the ATLAS simulation

[1] We are grateful to Andrea Dell'Acqua for providing the code for this.

[2] We do not consider here the facts that, even in the absence of escaping neutralinos, the production of hard neutrinos from SUSY decays is a potentially important source of missing energy, and that the slow nature of the staus may be the cause of a momentum imbalance for the triggers.

software are not yet ready for physics studies [3]. Although the ATLAS LVL1 trigger configuration is not finalized, we are very interested in even these preliminary results, as the LVL1 trigger will make by far the largest reduction of the event rate. The final trigger thresholds will necessarily depend on the rates actually found in the experiment, so the setup used in this study is the default LVL1 trigger menu `CSC-06` in `ATLAS` release `12.0.6`.

The efficiency found for the various LVL1 triggers for supersymmetric events in each of the three benchmark scenarios is displayed in Fig. 3 (left). From left to right are shown: triggers from energy clusters in the electromagnetic calorimeter (`EM`), muon triggers (`MU`), jet triggers (`JT`) and tau triggers (`TAU`). Numbers represent the required threshold in GeV, and 'i' represents an isolation requirement for a cluster [4]. The number of these triggers per event are very large, but do not give a realistic picture of the trigger rate, as most of these triggers will be heavily prescaled, if they exist at all, even at the expected first-year luminosity.

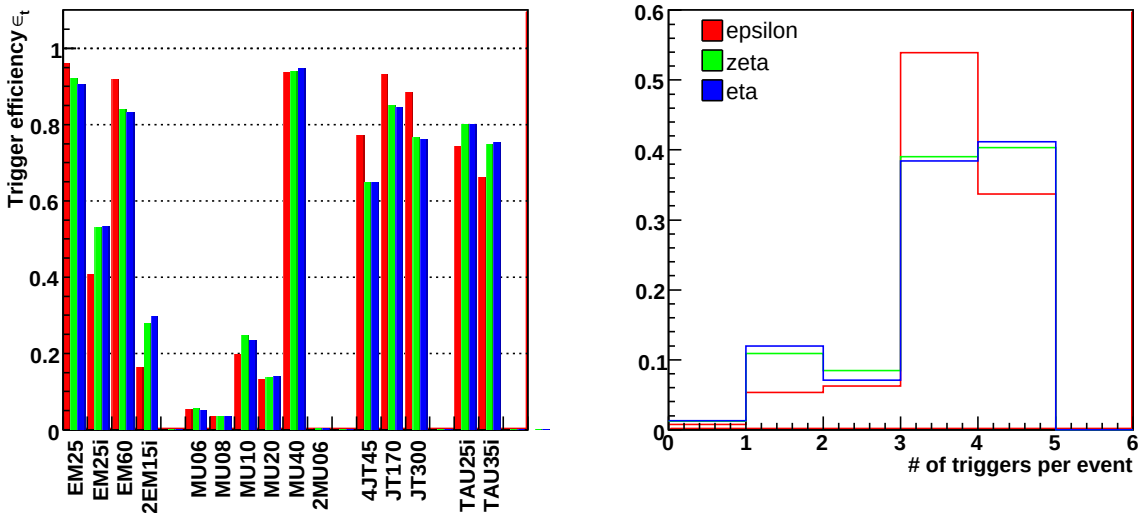

Figure 3: The efficiencies of various LVL1 ATLAS triggers for the three benchmark points (left), and the total number of LVL1 triggers per event in the restricted trigger selection described in the text (right).

Another important issue should also be noted when interpreting these results. The current status of the simulation of LVL1 muon triggers for slow-moving staus is not completely realistic. Staus which deposit hits in the three RPC layers, but are so slow that the timing of the hits are in different bunch crossings, because of the long ToF of a semi-relativistic particle through the layers, will not be triggered on in normal ATLAS running. For most supersymmetric events this trigger problem is not very important, because such slow staus account for only a small fraction of the full spectra [5]. We can see from Fig. 1 (left) that the fraction of staus with $\beta\gamma < 1.0$ is between 11% and 18% for the different benchmarks. However, for Drell-Yan production, where

[3] However, we do not expect important decreases in the total trigger efficiencies when the higher-level triggers are implemented, for the reasons to be described below.

[4] Note that in the present software a single muon can give only one trigger, i.e., if it is above more than one threshold for an object of its type, only the highest-threshold trigger is registered. However, there may be more than one muon trigger in an event, as there may be several muons.

[5] Staus with $|\eta| \approx 1$ have the longest distance to travel between RPC layers. Given a 25 ns gap between bunch crossings and a distance of ≈ 15.5 m to the outer RPC layer, the critical velocity is $\beta = 0.67$, or $\beta\gamma = 0.9$, ignoring any significant energy loss.

the staus are the only source of triggers, this effect may be very important, and could lead to a significant reduction in the trigger efficiency. This is even more likely to be the case because these staus are in general slower, as is seen from Fig. 2 (left), lacking the boost given by the decay of heavy sparticles.

To estimate the effect of this problem with the trigger simulation we disregard all muon triggers, with the exception of `MU40`, which is not expected to be prescaled. For the `MU40` trigger we also require the presence of at least one stau with $\beta\gamma > 0.9$ or muon with $p_T > 40$ GeV in the event truth record, and within the muon trigger geometric acceptance of $|\eta| < 2.4$, to register the trigger. Because of the lack of identification of the triggering object in the present simulation code, there is a possible effect from erroneously accepting a trigger because it belongs to a stau under the given threshold, in the same events as a stau or muon over the threshold, but not triggering. We have therefore made a cross check of events with one and only one stau above threshold, and find that these have a high efficiency for the `MU40` trigger alone of 85.5%, which implies that this effect is small.

Our treatment of the LVL1 muon triggers is conservative, and because of the need for making model-independent searches and setting exclusion bounds from the absence of Drell-Yan events with massive metastable charged particles, the subject of muon triggers and slow particles is very important, and should be studied further in the future, when a more realistic trigger simulation is possible.

Further taking into account the large prescaling of the triggers shown in Figure 3 (left), we disregard all tau triggers, limit the electromagnetic calorimeter triggers to `EM25i` and `EM60`, and use only the hardest jet trigger `JT300`. Even with these limitations on the triggers, we find that for the ϵ point we have on average 3.14 triggers per event in the LVL1 trigger simulation, with an overall trigger efficiency of 99.2%, which demonstrates that our expectations of high trigger efficiencies are borne out in the LVL1 triggers. In Fig. 3 (right) we show the distribution of the number of triggers per event under the restricted set of triggers. It is these trigger requirements that will be used in our final determination of the stau mass in Section 8.

For the other two benchmark points, the heavier squarks and gluinos have lower production cross sections and a much larger fraction of events are due to stau pair production or associated neutralino/chargino production. It is natural to expect that this will lead to less activity per event, and hence to lower trigger rates. From Fig. 3 (left) it is evident that these benchmarks have less activity in the important hard jet triggers compared to ϵ. The `EM` and tau triggers maintain good efficiency. In particular the isolated calorimeter triggers improve for these benchmarks, due in part to the production of electrons from gaugino decays and in part to the decays of taus produced from neutralino decays,[6] where in both cases the higher masses of the initially-produced sparticles give harder Standard Model decay products. The muon triggers are very similar for all three benchmarks. The final result is only a small decrease in the total trigger efficiency with respect to the ϵ benchmark point. The total trigger efficiencies at LVL1 are 98.8% and 98.7% for the ζ and η points respectively, while the average number of triggers are 3.06 for both points. At our current level of understanding of the LVL1 triggers, this implies that there will be no problem triggering on supersymmetric events for the benchmarks in question.

It was pointed out in [45] that the read-out of detector sub-systems is tuned to particles moving close to the speed of light, and that, for a very slow-moving particle, this may mean that information is lost, even for triggered events, if the read-out of the non-triggering sub-systems do not take this possibility into account. We join in the request of the authors of [45] that this issue be considered in the ongoing optimisation of the ATLAS data-acquisition system, which will

[6] The process $\tilde{\chi}_1^0 \to \tilde{\tau}_1\tau$ is the dominant decay mode for the lightest neutralino for all three benchmark points [39].

also include the specification of the higher-level triggers. However, we believe that the analysis of this Section gives good reason to think that interesting analyses will be possible even when realistic higher-level triggers are taken into account.

4 Reconstruction of Stau Tracks

In order to identify massive metastable charged particles in ATLAS, such as the staus of our benchmark points, we need to reconstruct their high-p_T tracks in the muon system and separate them from muons, either via their low velocities or because their ionisation rates are incompatible with muons. Before we can do either, we first face here the initial problem of reconstructing tracks from slow-moving staus.

The ATLAS muon system naturally has a very good track reconstruction efficiency for muons, which in good regions is close to 100% for muons with $p_T > 6$ GeV. However, this is not the case for the staus. One important generic difficulty with the reconstruction of a stau is its late arrival time in the muon system following a trigger decision, compared to a muon with the same momentum. Fortunately, once an event has passed the LVL1 trigger, data from the MDTs corresponding to the ~ 700 ns after the trigger bunch crossing are extracted from the pipe-line memories, providing a window for catching particles in the muon system. In the track fitting the recorded drift-times of the MDTs are converted to drift circles, assuming the arrival time of a relativistic particle. For slow-moving particles, this will lead to an error in the drift-circle calculation and a degradation of the fit quality for low β. Indeed, below a certain velocity threshold the error will be too large to reconstruct tracks at all. While varying the offset of the arrival time in a track re-fit to improve the fit quality can itself be used to measure the velocity of the particle [35], the initial track identification is difficult to improve in this manner, since it would in principle require trying to fit all possible tracks through all MDT hits, with all possible arrival times. Other important problems in the stau track reconstruction include the large energy loss due to ionisation at low velocities, which pushes the velocity further down, and also the significant effects of multiple scattering as a result of the large stau mass. Thus one expects to lose a significant fraction of the tracks of slower staus.

Using the reconstructed tracks, we can plot the reconstruction efficiency of the staus as a function of velocity, $\beta\gamma$, and detector geometry, characterized by the pseudo-rapidity η, neglecting trigger effects. When evaluating the efficiency, we require combined ID and muon system tracks matched to a true stau within a cone of $\Delta R < 0.2$. The requirement of an ID track means that we only take into account staus with $|\eta| < 2.5$. We see from Fig. 1 that this requirement is rather insignificant, excluding less than 1% of the staus. Results for all three benchmark points are shown in Figure 4.

In the left plot, which shows the efficiency as a function of $\beta\gamma$, we see a stable plateau with a reconstruction efficiency of $\sim 80\%$ for $\beta\gamma > 1.2$. Below this value, as expected, the efficiency decreases rapidly for the slower staus, because of problems with the drift circles and because of increasing energy loss due to ionisation and multiple scattering at low velocities [7]. We see that the efficiency for ζ and η is slightly below that of ϵ, except at the lowest velocities. This effect is yet to be understood.

In the right plot of Fig. 4, which displays the efficiency as a function of pseudo-rapidity, there are clearly visible 'holes' in the muon system efficiency. These occur where expected, most

[7] Looking at the amount of material traversed in the calorimeters and the energy lost due to ionisation, as calculated from the Bethe-Bloch formula, one can estimate a lowest possible velocity for a stau to be able to enter the muon system. This yields values of $\beta\gamma \approx 0.45$ for ϵ, and $\beta\gamma \approx 0.36$ for ζ and η, consistent with the results of the simulation in Fig. 4.

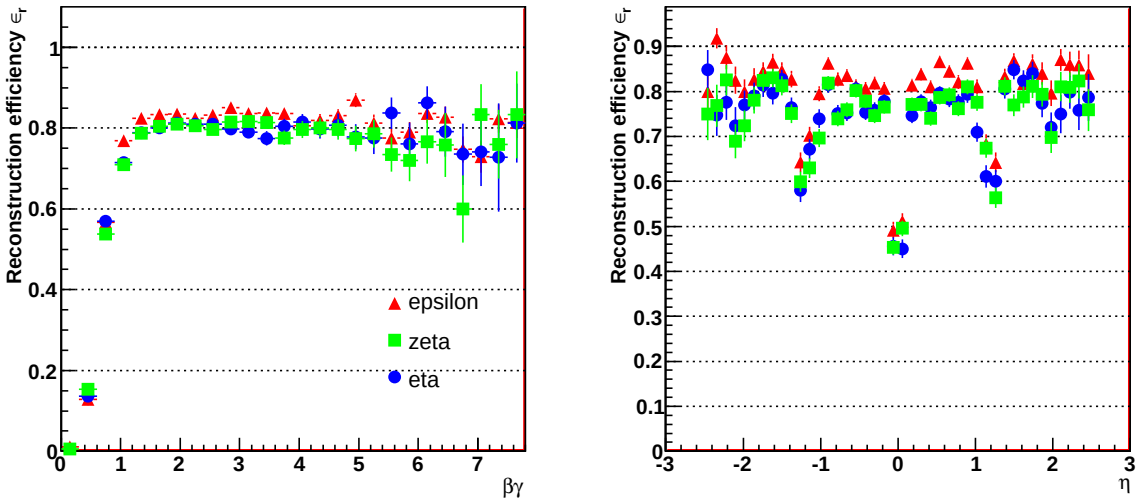

Figure 4: The stau track reconstruction efficiency for the ϵ, ζ and η benchmark points as a function of $\beta\gamma$ (left) and pseudo-rapidity η (right).

notably at $\eta \approx 0$, where the ATLAS muon spectrometer has a gap for cables and other services. The 'holes' at $|\eta| \approx 1.3$ have similar causes. Even more so than for the left plot, the efficiency for ζ and η is consistently below that of ϵ. This is to be expected from Fig. 1, where we see that benchmarks ζ and η yield larger fractions of staus with velocities below $\beta\gamma = 2.0$.

5 Momentum Measurement

In order to measure the mass of the stau, one needs to determine both its velocity and momentum. However, there is some tension between the measurements of velocity and momentum in the muon system for a given stau mass. The velocity precision in general increases with increased ToF - until one approaches the limit where it becomes impossible to identify a track - while the precision on the momentum measurement is mostly flat, before it deteriorates more rapidly than the velocity measurement at low velocities. The expected velocity precision make the staus with the lowest momenta very interesting and, in order to measure better the momenta, we utilise here information from both the muon system and the ID, using the combined fits of tracks from hits in both sub-detectors.

For relativistic staus, hits in the Monitored Drift Tubes (MDTs) give precise measurements of the momenta at the level of accuracy of muon measurements, mostly limited by the sagitta measurement error. However, at low β, problems with the bias of the drift circles, as discussed in the previous Section, and also multiple scattering, considerably reduce the precision of the MDT measurements. This can be seen in Fig. 5, where we plot the momentum resolution as a function of momentum for staus produced in our simulations of the ϵ and ζ benchmark points, using only events passing the restricted triggers of Section 3. This and other distributions for η are similar to those of ζ.

From Fig. 5 we can see that the ID is complementary to the muon system for the non-relativistic staus that are of special interest here. In particular, the inclusion of the ID gives us a significant advantage at low momenta for the ζ benchmark point with its heavier stau. Although the ID performs better than the drift circle measurements of the MDTs at low momenta, the ID

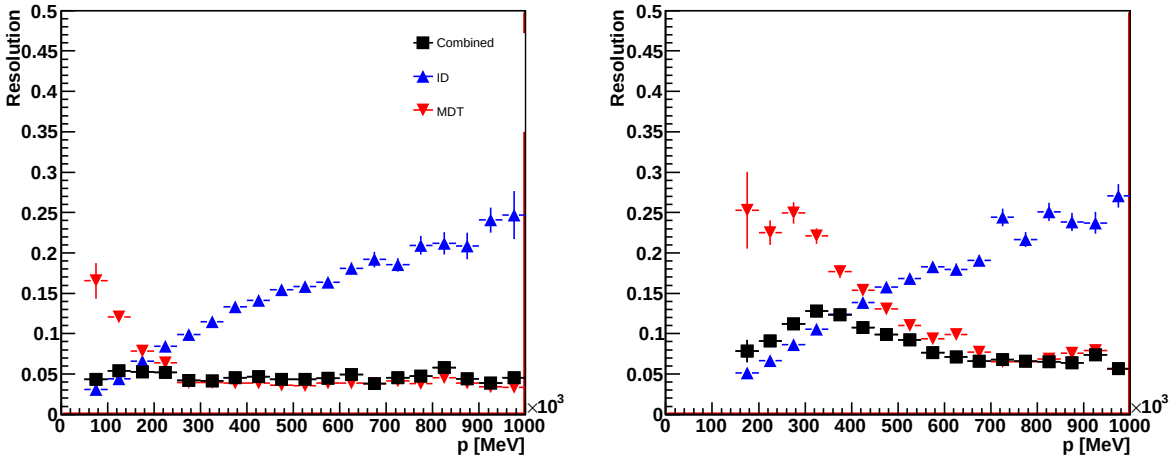

Figure 5: The $\tilde{\tau}_1$ momentum resolution for the ϵ (left) and ζ (right) benchmark points as a function of the true momentum. We show separately the resolutions of the muon system (red), the inner detector (blue) and the combined fit (black).

tracking system has more limited precision for measuring high momenta, because of its restricted geometry and hence the small sagittae of the tracks.

In the combined fit ID tracks are matched to a muon system track and refitted, using the MuID package. The combined fit performs extremely well, with a very flat distribution as a function of momentum, and with a resolution of slightly better than 5% for ϵ. Comparing the results of the two benchmark points shown, we see that the benchmark ζ, with its heavier stau mass, has a worse resolution, in particular for the lower momenta. This is to be expected since, for a given momentum, the velocity of the stau is smaller.

When compared to the results of [35], we find that the combined fit performs better for the ϵ benchmark point over much of the high momentum range, down to ≈ 300 GeV where the advantage of the track refit performed in [35] becomes important for the slowest staus. The effect of including the ID again outperforms the improvements of the refit for the lowest reconstructed momenta at ≈ 100 GeV where the MDT measurement becomes particularly bad. In terms of a comparison to the parametrisation of the stau momentum resolution given in [35] and used in [39], Section 3.1.2 and Eq. (3.1) respectively, we find for the ϵ benchmark point parameter values of $k_1 = 0.0060 \pm 0.0001$ for the sagitta measurement error and $k_3 = 685 \pm 16$ for the error due to energy loss in the calorimeters. However, the effect of including the ID in the track fit changes the shape of the resolution to the point where this particular parametrisation results in a bad fit.

6 Time-of-Flight Measurements

While the stau momentum may be taken directly from a track fit, as discussed in the previous Section, one needs to measure the Time-of-Flight (ToF) of the stau in order to determine its velocity. One may infer the ToF indirectly by performing a re-fit of the muon track while changing the assumed arrival time in the MDTs, as briefly mentioned in previous Sections and studied in [35], or one may measure directly the ToF using the time-stamps of hits in the RPCs. Here we consider the latter method.

The naive approach to measuring the velocity of a stau would be to use the distance of an

RPC hit from the interaction point, and divide by the ToF measured in the RPC to arrive at a velocity. While this is in principle a much cleaner measurement of velocity than that obtained from a re-fit of a track, there are important sources of systematic error. In particular, to calibrate properly the velocity measurement, we must take into account effects of the geometry of the detector and the properties of the RPCs.

The RPCs have a very limited spatial resolution of $\sim$ 1 cm, and therefore serve only as triggers and as seeds for the precision track fit to MDT hits in the muon system. Due to their trigger role, the RPCs do however have excellent time resolution, sampling the signal every 3.125 ns, and with a resolution of 0.9 ns. In addition, there is an intrinsic time jitter of $\sim$ 1.5 ns in the electronics, which we include in the simulation, but even so this gives an impressive total time resolution of $\sigma_t = 1.75$ ns. The RPC elements are only read out at one end and, with a typical element length of $\sim$ 1 m and a propagation speed of $\sim$ 200 mm/ns, there is a signal delay significantly larger than σ_t, leading to an underestimation of the velocity. This delay affects, in particular, the high-velocity tracks whose recorded time is smallest, and is simulated in the current software. To correct for this delay, we use the track prediction to arrive at the actual crossing point of the particle. From the distance to the read-out we can calculate the expected propagation delay and subtract this from the measured time.

Due to the bending of the tracks in the magnetic field, the distance travelled by a particle is also slightly longer than that of a straight line from the interaction point. Again this causes an underestimate in the naive velocity calculation. This affects, in particular, the slowest staus. Taking this into account we integrate the distance travelled along the fitted track, and use this length when calculating the velocity.

To demonstrate the effects of our calibration, we plot in Fig. 6 the true velocities β for the staus at the interaction point, versus the measured velocities for individual RPC hits in our full simulation samples for ϵ (left) and ζ (right), both before and after the calibration is performed. The RPC hits used are those that belong to combined muon system and ID tracks, with some further requirements on track quality and RPC hits that are given in Section 7. The expected underestimation of velocities is seen in the uncalibrated sample, which the calibration efficiently corrects for at the highest velocities. However, we also see that, in particular for ϵ, the velocities of the staus at low β is underestimated even after adjusting for the signal propagation delay and the bent track. This is caused by the increasing amounts of energy lost from traversing the calorimeters at lower velocities, which should be re-calibrated by looking at the energy deposited around the track. Due to the present status of the ATLAS software for combining tracking and calorimetry, it has not yet been possible to do this. For ζ, the higher mass leads to a smaller fractional energy loss for comparable velocities. The results for η are very similar.

In Fig. 7 we show the resulting resolution on the velocity measurement, again for ϵ and ζ and for RPC hits on tracks picked as in Fig. 6. The resolution is shown both for single RPC hit measurements, and for averages over all hits assigned to a reconstructed track. Both improve with lower velocity, down to $\beta = 0.5 - 0.6$, where there are few events, and where track reconstruction becomes difficult. The single RPC hit measurements exhibit a clear linear behaviour of the resolution with β down to these values. The track measurements are significantly better at high velocities, but improve less as the velocity is lowered. The large errors on some bins at low velocity are the results of a combination of low statistics and some measurements that lie far from the nominal value. Compared to the results of [35] the velocity resolution for tracks at the ϵ benchmark point is consistently better using RPC hits than with the track refit method, at least down to $\beta \simeq 0.6$ where our statistics are low. Again the results for η are comparable to ζ.

For the RPC velocity measurement to work in an optimal way in ATLAS, it is vital that the signal delay can be adjusted in an accurate manner, and that energy-loss effects are well

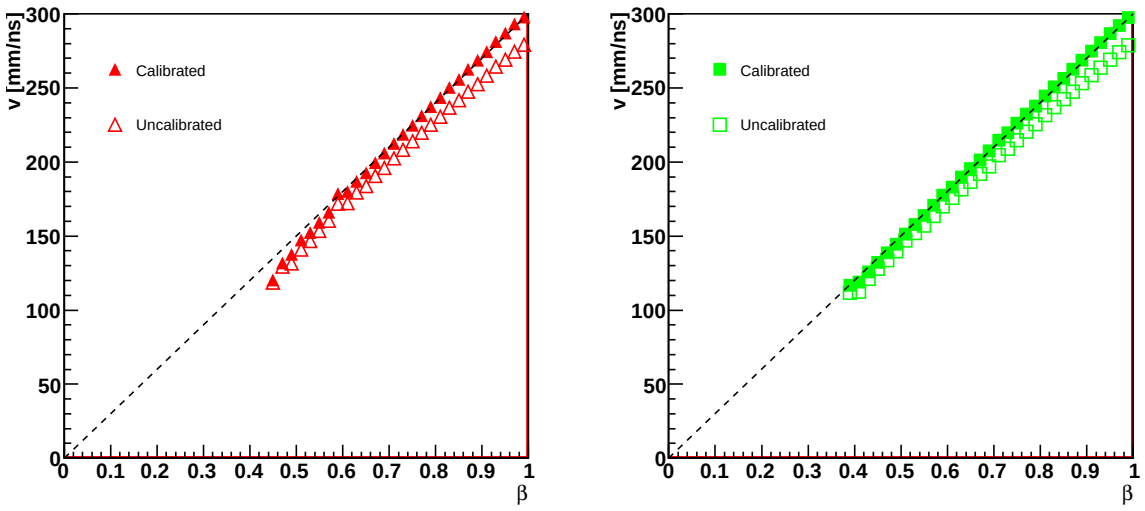

Figure 6: The velocity measured using RPC hits versus the true MC velocity β of staus at the interaction point, for the ϵ (left) and ζ (right) benchmark points. We show the uncalibrated results (open symbols) and the calibrated velocities (closed symbols). We also show the nominal relationship (dashed line).

understood. However, despite the deviation due to energy loss, these results show that we can measure stau velocities and recalibrate detector effects with good precision over a large range of velocities. We expect to be able to make further improvements by adjusting for energy loss in the calorimeter once the ATLAS simulation software advances sufficiently. Having determined the stau velocity, we may now plot the measured momentum versus $\beta\gamma$ to find the stau mass from Eq. (1). This is discussed in Section 8 where we combine all of the effects we have studied.

7 Background Simulation

As we have seen, the distinctive signature of GDM models is a pair of slow-moving muon-like objects, namely the staus at the end of every sparticle decay chain. To separate GDM events from Standard Model events with a real muon pair, we can use the velocity information found in the previous Section. All real muons passing the basic ATLAS reconstruction requirement of $p_T \gtrsim 6$ GeV will be highly relativistic and have an insignificant ToF delay compared to $\beta = 1$, barring possible mis-reconstruction and mis-identification. In order to estimate the effects of backgrounds on our stau benchmark samples we have examined muons already present in the supersymmetry samples, and a Z+jet sample with forced $Z \to \mu^+\mu^-$ decay. This sample was generated, simulated and reconstructed in the same manner as our supersymmetry samples, with an additional cut of $p_T > 50$ GeV imposed on the partons in the generation of the hard interaction [8], simulating in all 9599 events produced by PYTHIA [40]. According to the NLO cross section of 162 pb calculated with MCFM [46], this corresponds to an integrated luminosity of 59.3 pb^{-1}.

We impose some basic cuts on the stau candidate tracks used in our analysis, so as to isolate them from background muons. As mentioned previously, we use only combined ID and muon

[8] Later we require two stau candidates with $p_T > 70$ GeV in each event, which should justify this restriction.

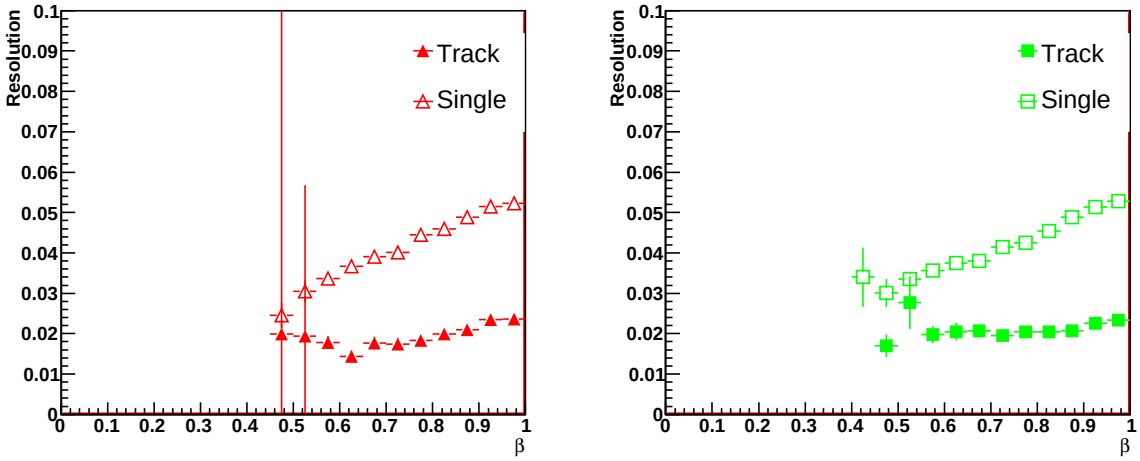

Figure 7: The resolution of the velocity measurement using RPC hits as a function of the true MC velocity β of staus at the interaction point, for the ϵ (left) and ζ (right) benchmark points. We show separately the results from single hits (open symbols) and velocity averages for reconstructed tracks (closed symbols).

tracks, and we require a LVL1 trigger for the corresponding event from our very restricted list of triggers. We also require that:

- the track fit has $\chi^2/\mathrm{ndf} < 2.0$,
- there are at least four RPC hits on each track,
- the tracks are reconstructed with $p_T > 70$ GeV.

Due to the trapping of the slowest staus discussed above, the momentum cut should not remove any significant signal. In the Z+jet sample a total of only 2161 muon track pass these cuts, giving an efficiency of $10.9 \pm 0.2\%$. While this is a dramatic reduction compared to the signal efficiency, which after these cuts and trigger requirements is down to $47.6 \pm 0.4\%$ (for ϵ), this is by far insufficient to separate the staus from background events.

In Fig. 8 we compare the measured $\beta\gamma$ for staus and muons in the supersymmetry events generated for the ϵ, ζ and η benchmark points and muons from the Z+jet sample. We note that the velocity distributions for the muons in the supersymmetry samples are quite similar to the muon distribution for the Z+jet sample, indicating that the velocity (mis)measurements of the muons have fairly universal characteristics. If we now cut on the measured velocity of the tracks, requiring $\beta\gamma < 5.0$, we increase the signal to background ratio further. The efficiencies obtained for the stau and muon tracks in the various samples after this cut are shown in the third column of Table 1. In the next two columns we show the number of surviving events when we require one or a pair of these tracks in an event, all results having been rescaled to an integrated luminosity of 1 fb^{-1}. For the Z+jet sample, there are only two events left after the two track requirement, thus the given statistical error is large.

We conclude that with this simple cut on the measured velocity the number of surviving Z+jet background events is small for the ϵ benchmark point, and on the order of the supersymmetry signal for the other two benchmarks, depending on the exact value of the velocity cut. There are of course many other potential SM backgrounds producing muons that could

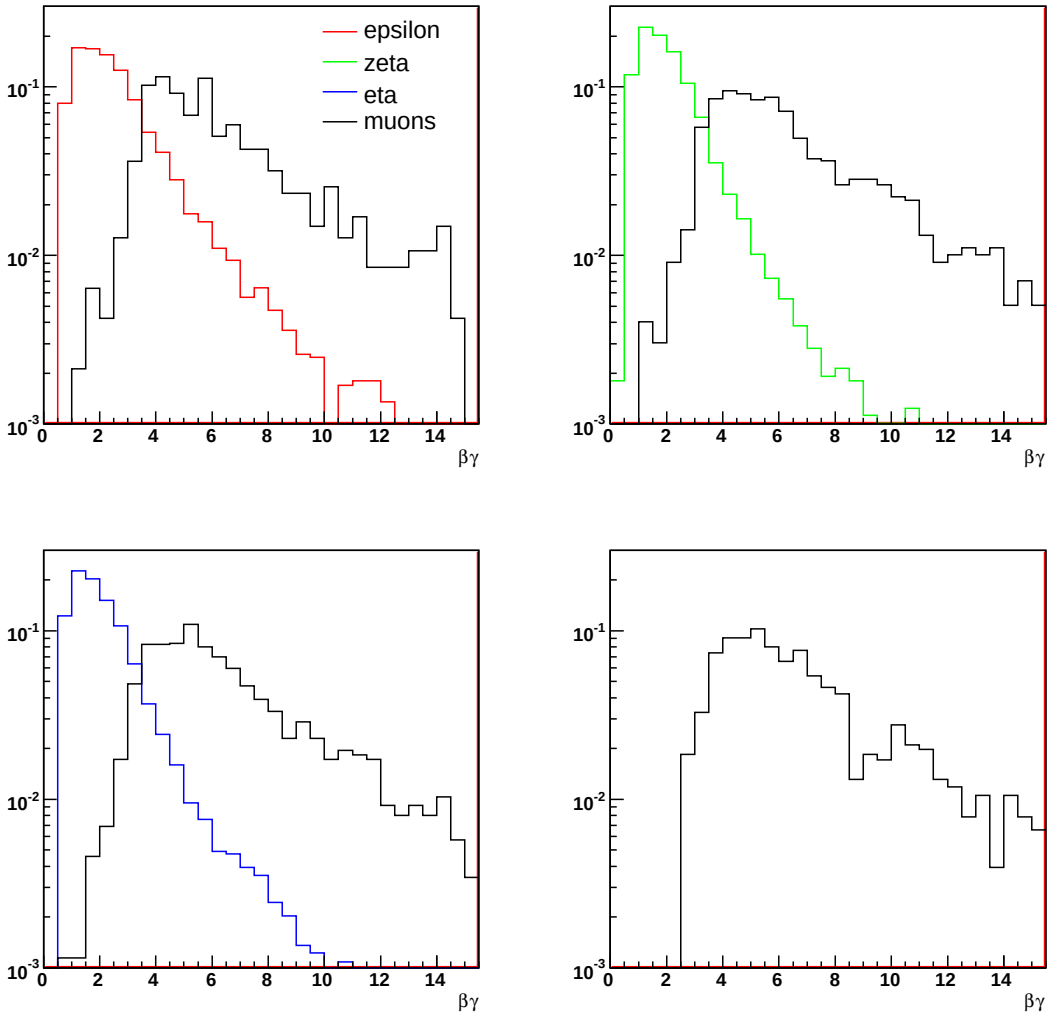

Figure 8: The distributions of the measured velocity $\beta\gamma$ for staus (colour) and muons (black) for the ϵ (top left), ζ (top right), η (bottom left) and Z+jet samples (bottom right).

be mis-measured, or even fake muon tracks. We have checked the Z+jet sample for muons candidates that do not originate from the Z decay, and find that none of these survive the track cuts given above. This is not surprising considering the high transverse momentum requirement. Similarly we have searched for muons candidates faked by the hadronic activity in the events. No muon tracks survive the cuts that are not well matched to a true muon. The result is thus the same, due to the large momentum cut no fakes are present. It is beyond the scope of this paper to attempt a complete investigation of all of these possibilities for the numerous SM backgrounds, particularly in view of the necessary large-scale event production, but this should be possible in the future with the use of larger samples of SM events produced within the ATLAS collaboration.

However, it is likely that a very good signal-to-background ratio such as that found here will survive. We give three main arguments in support of this optimistic outlook. First, as we have seen, the behaviour of the muons in all four samples was very similar. If this trend continues, the

Sample	Particle	Efficiency (in %)	One track	Two tracks
ϵ	$\tilde{\tau}_1$	41.55 ± 0.35	1537 ± 17	572 ± 13
	μ	3.15 ± 0.19		
ζ	$\tilde{\tau}_1$	44.24 ± 0.36	10.4 ± 0.1	5.1 ± 0.1
	μ	4.72 ± 0.20		
η	$\tilde{\tau}_1$	44.19 ± 0.39	10.6 ± 0.1	5.3 ± 0.1
	μ	4.67 ± 0.21		
Z+jet	μ	1.87 ± 0.10	3881 ± 253	34 ± 24

Table 1: Efficiency of the velocity cut $\beta\gamma < 5.0$ for the three benchmark points and the Z+jet sample. The track cuts give the remaining number of events corresponding to a 1 fb^{-1} sample.

muon background velocity distribution is simply a cross-section-dependent rescaling of Fig. 8 (right), which implies that the cut on velocity should be just as effective. The second reason is the existence of additional cut variables we have ignored. We have not looked at the energy deposits around the tracks in the calorimeters, which should be substantially larger than for muons. The same should be true for the amount of ionisation in the MDTs, which has been studied for this purpose in [47]. Also, we have the possibility of lowering the velocity cut further from our rather conservative value of $\beta\gamma = 5.0$. Finally, in most of our signal events there are other distinguishing features inherent to supersymmetry, such as hard jets and leptons, that could be used to reduce backgrounds in the same manner as in other supersymmetric models. Also the SM backgrounds could be further reduced by using their distinguishing features, such as the di-muon invariant mass for a Z.

8 Determining the Stau Mass

In this Section we give our final estimate of the accuracy achievable in ATLAS for measuring the stau mass at each of the three benchmark points using timing information from the RPCs. For the stau tracks used we require at least one LVL1 trigger in the event, using the restricted set of triggers discussed in Section 3. We further apply the cuts given in Section 7, in addition requiring two tracks with a velocity in the range $1.0 < \beta\gamma < 2.0$ to remove the Standard Model background, the remnant of which has a negligible effect on the stau mass estimates. From the identified stau tracks we calculate the corresponding mass using Eq. (1) and plot the results in Fig. 9 for the ϵ (left), ζ (centre) and η (right) benchmark points.

We have made Gaussian fits to the mass peaks. The resulting masses, statistical errors and nominal values for all three benchmark points are found in Table 2. For all three benchmark points we have very small statistical errors, in the order of 0.2%. For the ϵ benchmark point this is the result for statistics comparable to that expected for the first year of LHC running, while for the other two benchmark points this statistics corresponds to the long-term potential of the LHC. This can be compared to the results of [35, 36], where the accuracy expected for the stau mass measured with MDT information and track refits is in the same range for a light stau.

We observe some deviation from the nominal values caused by non-Gaussian tails in the mass distributions, clearly visible in Fig. 9 towards higher masses, and indicated by the less than perfect fit quality, in particular for η. This systematic error is primarily caused by a slight systematic shift of the measured stau momentum away from the true momentum and towards higher momenta, increasing with momentum, and is at the level of $0.5 - 1.0\%$ for the three benchmarks. We have found that narrowing the velocity range included in the fit towards

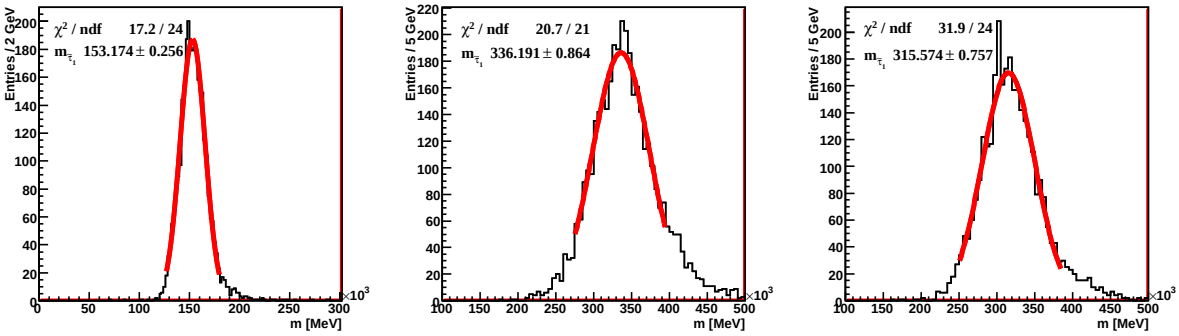

Figure 9: Histograms of stau mass determinations for the ϵ (left), ζ (middle) and η (right) benchmark points.

slower staus improves both the fit quality and the systematic shift in masses, at the expense of larger statistical errors. With a careful recalibration of stau momentum it seems possible to remove at least part of the systematic error. The refit of tracks assuming lower velocities, as demonstrated in [35], may also be of considerable use here in improving the momentum measurement. The exact details of such a combined procedure should be the subject of further study.

Sample	Mass	Nominal mass
ϵ	153.174 ± 0.256	152.475
ζ	336.191 ± 0.864	338.114
η	315.574 ± 0.757	318.931

Table 2: Measured stau masses, statistical errors and nominal values for the three benchmark points

9 Conclusions

We have investigated the use of the ATLAS RPCs in measuring the masses of massive metastable charged particles in a full simulation of the ATLAS detector, using three GDM benchmark scenarios with metastable staus as our test cases. The benchmark points used represent widely different production cross sections at the LHC, and a significant range in stau masses.

We find that the ATLAS LVL1 triggers retain our signal events efficiently, even after conservative assumptions on the use of the muon triggers for slow moving staus we have trigger efficiencies in the range of $98 - 99\%$. We also find a high reconstruction efficiency of $\sim 80\%$ for stau tracks, using a combined fit to hits in the ID and the muon system. The combined track fit also gives a good determination of the stau momentum over a large range of momenta, improving significantly on the stand-alone muon system results at low momenta.

We further find that the RPCs can be used to determine the velocity of the staus with excellent precision, with a resolution of $\sim 5\%$ for all velocities. This method is complementary to the technique already studied, where the velocity is measured by a refit of tracks in the muon system [35]. In particular it improves significantly the velocity measurement for the faster staus. The relatively low velocity of a significant fraction of the staus enables us to make a very efficient

SM background cut, requiring two slow "muon-like" tracks in each event. We have tested this cut on a sample of Z+jet events, finding that a threshold of $\beta\gamma < 5.0$ effectively removes the background for the ϵ benchmark, while it significantly reduces the background for the other two benchmark points.

The RPC velocity measurements of the staus, taken together with the momentum measurements from the combined muon system and ID tracks, enables us to measure the stau mass with a statistical accuracy of 0.2%, for a number of events corresponding to the first year of running of the LHC for the ϵ benchmark point, and for a number of events expected to be the ultimate reach of the LHC for the ζ and η benchmark points. We expect this optimistic conclusion to survive the realistic implementation of the higher-level ATLAS triggers. It is encouraging that the ATLAS detector and software, which was not designed with the detection of a metastable massive particle in mind, nevertheless has an excellent capability for detecting and measuring such a particle.

10 Acknowledgements

This work has been performed partly within the ATLAS Collaboration, and we thank collaboration members for helpful discussions. We have made use of the physics analysis framework and tools which are the result of collaboration-wide efforts. We particularly thank Bjarne Stugu and Giacomo Polesello for helpful discussions on a number of topics. We thank Andrea Dell'Acqua for providing the `GEANT4` implementation of the stau for the full simulation. ARR acknowledges support from the European Community through a Marie Curie Fellowship for Early Stage Researchers Training.

References

[1] L. Maiani, *All You Need To Know About The Higgs Boson*, in Proceedings of the Gif-sur-Yvette Summer School On Particle Physics, 1979, pp.1-52.

[2] G. 't Hooft, in *Recent Developments In Gauge Theories. Proceedings, Nato Advanced Study Institute, Cargese, France, August 26 - September 8, 1979,* eds. G. 't Hooft, C. Itzykson, A. Jaffe, H. Lehmann, P. K. Mitter, I. M. Singer and R. Stora, (Plenum Press, NY, 1980).

[3] E. Witten, Phys. Lett. B **105** (1981) 267.

[4] J. R. Ellis, S. Kelley and D. V. Nanopoulos, Phys. Lett. B **249** (1990) 441.

[5] J. R. Ellis, S. Kelley and D. V. Nanopoulos, Phys. Lett. B **260** (1991) 131.

[6] U. Amaldi, W. de Boer and H. Furstenau, Phys. Lett. B **260**, 447 (1991).

[7] C. Giunti, C. W. Kim and U. W. Lee, Mod. Phys. Lett. A **6**, 1745 (1991).

[8] H. Goldberg, Phys. Rev. Lett. **50** (1983) 1419.

[9] J. R. Ellis, J. S. Hagelin, D. V. Nanopoulos, K. A. Olive and M. Srednicki, Nucl. Phys. B **238** (1984) 453.

[10] M. Dine and W. Fischler, Phys. Lett. B **110**, 227 (1982).

[11] L. Alvarez-Gaume, M. Claudson and M. B. Wise, Nucl. Phys. B **207**, 96 (1982).

[12] C. R. Nappi and B. A. Ovrut, Phys. Lett. B **113**, 175 (1982).

[13] M. Dine and A. E. Nelson, Phys. Rev. D **48**, 1277 (1993) [arXiv:hep-ph/9303230].

[14] M. Dine, A. E. Nelson and Y. Shirman, Phys. Rev. D **51**, 1362 (1995) [arXiv:hep-ph/9408384].

[15] M. Dine, A. E. Nelson, Y. Nir and Y. Shirman, Phys. Rev. D **53**, 2658 (1996) [arXiv:hep-ph/9507378].

[16] G. F. Giudice and R. Rattazzi, Phys. Rept. **322**, 419 (1999) [arXiv:hep-ph/9801271].

[17] L. Randall and R. Sundrum, Nucl. Phys. B **557**, 79 (1999) [arXiv:hep-th/9810155].

[18] G. F. Giudice, M. A. Luty, H. Murayama and R. Rattazzi, JHEP **9812**, 027 (1998) [arXiv:hep-ph/9810442].

[19] J. R. Ellis, J. E. Kim and D. V. Nanopoulos, Phys. Lett. B **145** (1984) 181.

[20] T. Moroi, H. Murayama and M. Yamaguchi, Phys. Lett. B **303** (1993) 289.

[21] J. R. Ellis, D. V. Nanopoulos, K. A. Olive and S. J. Rey, Astropart. Phys. **4** (1996) 371 [arXiv:hep-ph/9505438].

[22] M. Bolz, W. Buchmuller and M. Plumacher, Phys. Lett. B **443** (1998) 209 [arXiv:hep-ph/9809381].

[23] T. Gherghetta, G. F. Giudice and A. Riotto, Phys. Lett. B **446** (1999) 28 [arXiv:hep-ph/9808401].

[24] T. Asaka, K. Hamaguchi and K. Suzuki, Phys. Lett. B **490**, 136 (2000) [arXiv:hep-ph/0005136].

[25] M. Bolz, A. Brandenburg and W. Buchmuller, Nucl. Phys. B **606** (2001) 518 [arXiv:hep-ph/0012052].

[26] M. Fujii and T. Yanagida, Phys. Rev. D **66**, 123515 (2002) [arXiv:hep-ph/0207339].

[27] M. Fujii and T. Yanagida, Phys. Lett. B **549**, 273 (2002) [arXiv:hep-ph/0208191].

[28] J. L. Feng, A. Rajaraman and F. Takayama, Phys. Rev. Lett. **91** (2003) 011302 [arXiv:hep-ph/0302215].

[29] W. Buchmuller, K. Hamaguchi and M. Ratz, Phys. Lett. B **574** (2003) 156 [arXiv:hep-ph/0307181].

[30] J. R. Ellis, K. A. Olive, Y. Santoso and V. C. Spanos, Phys. Lett. B **588** (2004) 7 [arXiv:hep-ph/0312262].

[31] J. L. Feng, S. f. Su and F. Takayama, Phys. Rev. D **70** (2004) 063514 [arXiv:hep-ph/0404198].

[32] J. L. Feng, S. Su and F. Takayama, Phys. Rev. D **70** (2004) 075019 [arXiv:hep-ph/0404231].

[33] L. Roszkowski, R. Ruiz de Austri and K. Y. Choi, JHEP **0508** (2005) 080 [arXiv:hep-ph/0408227].

[34] K. Hamaguchi, Y. Kuno, T. Nakaya and M. M. Nojiri, Phys. Rev. D **70**, 115007 (2004) [arXiv:hep-ph/0409248].

[35] G. Polesello and A. Rimoldi, ATLAS Internal Note ATL-MUON-99-06.

[36] S. Ambrosanio, B. Mele, S. Petrarca, G. Polesello and A. Rimoldi, JHEP **0101** (2001) 014 [arXiv:hep-ph/0010081].

[37] A. De Roeck, J. R. Ellis, F. Gianotti, F. Moortgat, K. A. Olive and L. Pape, arXiv:hep-ph/0508198.

[38] J. Polonyi, Budapest preprint KFKI-1977-93 (1977).

[39] J. R. Ellis, A. R. Raklev and O. K. Oye, JHEP **0610**, 061 (2006) [arXiv:hep-ph/0607261].

[40] T. Sjostrand, S. Mrenna and P. Skands, JHEP **0605**, 026 (2006) [arXiv:hep-ph/0603175].

[41] H. L. Lai *et al.* [CTEQ Collaboration], Eur. Phys. J. C **12** (2000) 375 [arXiv:hep-ph/9903282].

[42] M. Muhlleitner, A. Djouadi and Y. Mambrini, Comput. Phys. Commun. **168** (2005) 46 [arXiv:hep-ph/0311167].

[43] G. Duckeck *et al.* [ATLAS Collaboration], *ATLAS computing: Technical design report*, CERN-LHCC-2005-022.

[44] ATLAS Collaboration, *ATLAS: Detector and physics performance technical design report, Volume 1*, CERN-LHCC-99-14.

[45] S. Tarem, S. Bressler, E. Duchovni, L. Levinson, ATLAS Public Note ATL-PHYS-PUB-2005-022.

[46] J. Campbell and R. K. Ellis, Phys. Rev. D **65** (2002) 113007 [arXiv:hep-ph/0202176].

[47] P. Bagnaia, L. Menici, ATLAS Communications ATL-COM-PHYS-2005-007.